International Journal of Multiphase Flow 36 (2010) 682–689

Contents lists available at ScienceDirect

International Journal of Multiphase Flow

journal homepage: www.elsevier.com/locate/ijmulflow

Opposed bubbly jets at different impact angles: Jet structure and bubble properties

Francesc Suñol *, Ricard González-Cinca

Departament de Física Aplicada, Universitat Politècnica de Catalunya, Esteve Terradas 5, 08860 Castelldefels (Barcelona), Spain

ARTICLE INFO

Article history:
Available online 13 May 2010

Keywords:
Opposed jets
Two-phase flow
Bubble dynamics
Jet mixing

ABSTRACT

The structure of two colliding water jets containing small gas bubbles is studied experimentally. The effects of the separation distance between jets, as well as the orientation angle, on the spatial distribution of bubbles have been considered. Results on the global structure of the final jet and bubble properties have been obtained using a high-speed video camera, and measurements of the positions of coalescence events are presented. Jets are introduced through inclined pipes (with a diameter of 0.7 mm) into a large water tank to avoid wall effects. Inclination angle has been changed from 0° to 45° with respect to the horizontal, resulting in a 0° up to 90° impact angle between jets. Generation of bubbles is controlled by a T-junction device where a regular slug-flow is created prior to injection. Bubble sizes have been measured, and a mean diameter of around 1 mm has been obtained using high values of the liquid flow rate. In the studied range of separation distances between the bubbly jets, a more homogeneous dispersion of bubbles is created as the distance between jets is decreased and the momentum flux of each jet is increased. Higher numbers of coalescences are observed when using smaller distance between jets, and the obtained measurements revealed that the number of bubble coalescence events is reduced significantly using high values of liquid flow rates.

1. Introduction

The motion and interaction of gas bubbles in liquid flows have been extensively studied over many years, due to their fundamental importance in many multiphase systems. In the last decades, bubble jets have been the subject of theoretical and experimental studies since many applications such as aeration control or mixing devices require the use of small bubbles with high area–volume ratio. Bubble plumes are produced by injecting gas in a liquid tank, while bubbly jets are produced by injecting gas–liquid mixtures in liquids. This has additional advantages over the single phase injection, such as the production of bubbles with controlled size without the need of porous diffusers, low maintenance, and higher efficiency for gas transfer to the liquid phase (Lima Neto et al., 2008b). The sizes of the bubbles present in bubbly jets depend on the fluid properties, gas and liquid flow rates, and the geometry of the injection system. Varely (1995) investigated the bubble sizes in bubbly jets and found that bubble diameters decreases as the superficial liquid velocity increases, and the measured bubble size distributions were compared to normal, log–normal and gamma distributions. However, only size measurements were provided and no additional information such as bubble velocities or a study of the jet structure was described. An interesting investigation on the properties of bubbly jets injected in the vertical direction and horizontally has been carried out recently by Lima Neto et al. (2008a,b). In their work, the bubble properties and the liquid flow structure has been detailed for a single bubbly jet injected in a stagnant water tank, but the size of the bubbles is much higher than those reported in the present work.

On the other hand, the opposed-jet configuration has attracted special attention in the last decades due to its simple geometry and physical complexity. Opposed jets have been used extensively for studying turbulent properties of fluids (Eckestein et al., 2000; Chou et al., 2004; Eren, 2006; Weifeng et al., 2008) and the rich behavior of the flow concerning the structure of vortex interactions (Voropayev and Afanasyev, 1992; Afanasyev et al., 1995; Voropayev et al., 2003).

Many industrial applications have to deal with the improvement of fluid mixing efficiency, and some of them require a flexible control according to operation conditions. As investigated by Tsujimoto et al. (2006), such flexibility in the mixing processes can be achieved by changing the impact angle between the colliding jets: reducing the impact angle increases significantly the mixing efficiency. In this sense, the opposed-jet configuration with changeable orientation becomes an attractive method for enhancing mixing systems at low cost while maintaining high-efficiency and direct control.

An important area of applications of this kind of flows is the space industry. Small weight and more efficient thermal control are characteristics of two-phase systems which make them the appropriate candidates to replace single phase devices (Jianfu

* Corresponding author. Tel.: +34 934 134 156.
E-mail addresses: francesc@fa.upc.edu, francesc.sunol@gmail.com (F. Suñol).

0301-9322/$ - see front matter © 2010 Elsevier Ltd. All rights reserved.
doi:10.1016/j.ijmultiphaseflow.2010.03.009

et al., 2000; Ohta et al., 2002; Gabriel, 2007). On ground, when the density difference between the gas bubbles and the surrounding liquid is large, buoyancy plays an important role since it governs the dynamics of the mean flow. In space, where gravity can be neglected and no buoyant forces are present, many kinds of gas–liquid flows are still poorly understood. Additionally, the generation and injection of bubbles of controlled size in a microgravity environment is currently a challenging task. In the last few years, the bibliography on this subject has grown considerably, due to the increase of facilities for accessing microgravity platforms. For example, the reader may refer to Kim et al. (1994), Tsuge et al. (1997), Bhunia et al. (1998), Nahra and Kamotani (2003), Carrera et al. (2008), Arias et al. (2009) for interesting studies on bubble formation in low gravity. The understanding of the bubble behavior such as bubble generation or the structure of bubbly jets arises as one of the key points for the control of two-phase flows, both in normal and in low gravity.

In the present work we conduct an experimental study of the opposed-jet configuration, using gas–liquid jets, with different impact angles between jets and separation distances. The effect of the momentum flux J, which is indicative of the jet strength, has also been taken into account. The experimental setup, described in Section 2, is designed to study the behavior of such jets both on ground and in microgravity conditions. On ground results are presented in Section 3 in order to be compared with those obtained in a low gravity environment.

2. Experimental setup

The objective is to study the collision of two bubble jets on ground and in a microgravity environment, and the experimental setup is designed to be used in a drop tower facility (see Fig. 1).

On ground tests were conducted in a stainless steel rectangular tank with a length of 160 mm, width of 200 mm, and height of 250 mm, equipped with two methacrylate windows which allow the visualization of the bubble jets. The size of the test tank is large enough (compared to bubble diameter which is of order of 1 mm) to minimize any possible wall effects on the motion of the bubbles and the resulting jet structure. The test tank is initially filled with distilled and filtered water by a high-accuracy pump (Ismatec MCP-Z Standard) which takes the water from the liquid tank. A T-junction bifurcation is used to divide the liquid flow in two sub-lines that transfer the water to the bubble injectors (see operation description below in this section), ensuring an equal and constant flow rate for each sub-line. Liquid flow rates Q_L range from 15 ml/min to 30 ml/min for each injector, and are measured by a liquid flow meter (Bronkhorst L30). Gas (CO_2) is injected from a pressure bottle through a pressure controller (Bronkhorst P-702CV) and a choked orifice, setting the air flow rate Q_G from 5 ml/min to 20 ml/min for each injector. Gas flow rate is measured by an air flow meter (Bronkhorst F-201CV). Liquid and gas flow meters have an accuracy of 0.05 ml/min. Another T-junction bifurcation is used in the gas line to provide the air to each bubble injector. A residual tank is used to empty the excess of gas and liquid from the test tank, avoiding any risk of overpressure. The liquid and residual tanks are flexible high-resistance bags protected by rigid plastic boxes. Initially, the bag corresponding to the liquid tank is completely filled with distilled water while the bag corresponding to the residual tank is in vacuum.

The experiments were conducted at 20 °C and at ambient pressure. A high-speed video camera (RedLake MotionXtra HG-SE) is necessary to catch all bubble coalescence events and the individual bubble motions. Lighting was provided by a matrix of 280 ultra-bright LEDs and homogenized by a diffuser sheet. All the movies were recorded at 1000 fps with a resolution of 640 × 512 pixels (7 pixels correspond to 1 mm approximately), and post-processed by an image processing software. The basic experiment operations (full control of the gas and liquid lines, lighting and camera) can be controlled remotely from a computer via wireless, but the change of the impact angle φ and separation distances s between injectors has to be manipulated manually between two consecutive experiments. A schematic definition of φ and s is shown in Fig. 2.

The method used to generate the bubbles consists of a methacrylate T-junction with a diameter of 0.7 mm for each branch (see Fig. 3). Gas and liquid are injected at constant flow rates through the crossed capillary tubes of the T-junction, creating therefore a regular slug-flow with nearly fixed bubble size and generation frequency (Carrera et al., 2008; Arias et al., 2009). A capillary tube with a diameter of 0.7 mm and length larger than 70 mm carries the bubbles from the injector outlet to the test tank, ensuring stationary slug-flow conditions.

This method is insensitive to gravity force and is mainly dominated by capillary forces, since Bond number is very low

$$\mathrm{Bo} = \frac{\Delta\rho g d_C^2}{\gamma} < 1, \tag{1}$$

where $\Delta\rho$ is the density difference between the two phases, g is the acceleration of gravity, d_C is the capillary diameter and γ is the surface tension. With this property, the behavior of the injection device in low gravity is the same as on ground and we can fully characterize the operation of the injectors on Earth. An extensive range of bubble generation frequencies (up to 600 bubbles per second in the present study) can be achieved. Bubble sizes and velocities at the outlet of the injector are controlled by gas and liquid flow rates.

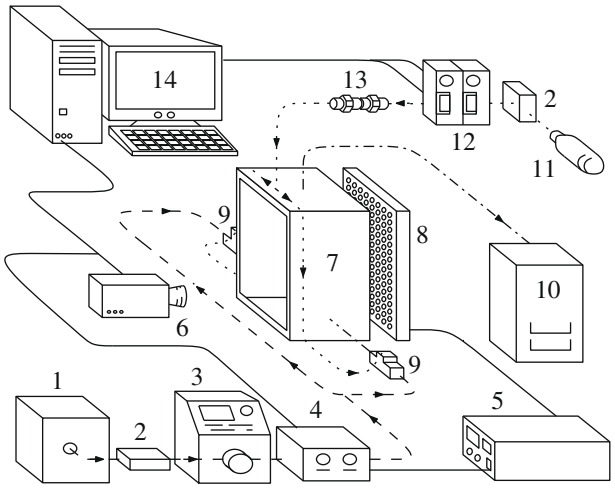

Fig. 1. Experimental setup. Solid lines: electric connections, dotted lines: gas tubes, dashed lines: liquid tubes, dash-dotted lines: gas–liquid tubes. 1: Liquid tank, 2: filter, 3: pump, 4: flow meter, 5: power supply, 6: HS camera, 7: test tank, 8: LEDs, 9: injectors, 10: residual tank, 11: gas bottle, 12: pressure controller and flow meter, 13: choked orifice, 14: PC.

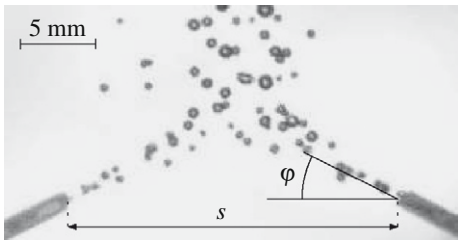

Fig. 2. Definition of the separation between injectors s and the impact angle φ.

Fig. 3. Illustration of the bubble generation method.

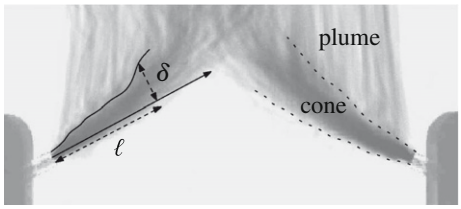

Fig. 4. Schematic definition of δ and ℓ.

The reader may refer to Carrera et al. (2008) and Arias et al. (2009) for a detailed study of this bubble generation method.

3. Results and discussion

In Fig. 2, a typical image of two colliding bubble jets generated at 30° with respect to the horizontal is shown. Different bubble sizes can be seen. These are due mainly to some coalescence events, although the performance of the injectors has also some influence on bubble diameters since they generate bubbles of a certain size with slight deviations.

This section has been divided in two parts: in Section 3.1 the attention has been focused on the jets structure as a whole, while in Section 3.2 the behavior of the individual bubbles that constitute the bubbly jets has been studied. In this second part, phenomena that do not perturb significantly the global structure of the jets are described.

3.1. Jet structure

According to Schlichting (1979), the momentum flux J can be regarded as the main parameter that characterizes the structure of single phase jets:

$$J = 2\pi\rho \int_0^\infty v_x^2 r dr, \tag{2}$$

where v_x is the liquid velocity at jet centerline and cylindrical coordinates (r,θ,x) are used. If we take into account both liquid and gas phases, J can be computed by

$$J = J_G + J_L = \frac{4}{\pi d_C^2}(\rho_G Q_G^2 + \rho_L Q_L^2) \tag{3}$$

where ρ_G and ρ_L are the gas and liquid densities, respectively. The momentum flux J is indicative of the jet strength, and most of the results presented in this work are based on this parameter. It is important to note that high values of J are necessarily due to high values of the liquid flow rate Q_L: increasing the gas flow rate Q_G results in a very small change in J since we have the parameter ρ_G multiplying the flow rate and $\rho_G \ll \rho_L$. This leads to the physical result of that smaller bubbles are created at higher momentum fluxes, while at lower values of J both the gas and liquid flow rates can contribute substantially to modify the momentum flux, and small and large bubbles can still be found.

Since the velocity of the bubbles inside the jets is very high, the human eye is not able to see the individual motion of those bubbles. Visually, two distinct regions are clearly observed (also observed by Lima Neto et al. (2008b) in their work of horizontal injection of gas–liquid mixtures in water): a bubbly cone emerging from the outlet of the capillary tube in the direction of injection, and a vertical bubbly plume in which the bubbles follow an approximately rectilinear path (see Fig. 4). In the first region, the jet strength is very high and is characterized by violent motion. Bubble dynamics are mainly dominated by inertial forces. Recorded movies show the paths of individual bubbles presenting some random oscillations typical of turbulent flows, and the shape of this zone is very similar to the conical shape of the single phase jet, but slightly deviated upwards in the vertical direction. On the contrary, the second region is formed by bubbles rising vertically at a constant and much slower velocity, the buoyancy is compensated by the drag force and no significant occurrence of coalescence events is observed. This bubbly plume is formed by bubbles that escaped from the bubbly jet, either by turbulent diffusion or by previously coalesced bubbles submitted to a strong buoyant force due to their larger size. It is important to note that the width of this bubbly plume is of the order of the separation between injectors, and in some cases of low impact angles with high values of J, the width of this bubbly plume is larger than the separation distance between injectors (as can be seen below in Fig. 9a and b).

As a first approximation, the separation between the cone and plume zones near the injection outlet can be considered a straight line that coincides with the aperture of the semi-angle of the conical bubbly jet. This approximation can be applied for a single bubbly jet, as done previously by Suñol et al. (2009). However, when dealing with the opposed-jet configuration, we have to take into consideration that the interaction between jets modifies the global resulting structure. In this perspective, the straight line approximation may not be valid anymore, and the length δ is defined as the distance between the injection axis and the point where bubbles start a vertical rise. The parameter δ will thus give information about the areas where the inertial forces become negligible. If a bubble is located above δ, its motion can be regarded as deterministic and is dominated by the buoyancy and drag forces. On the other hand, if a bubble is located below δ, the flow field is turbulent and it is mainly dominated by inertial forces. The distance δ is measured along the injection axis as can be seen in Fig. 4.

The variation of δ along the injection axis distance ℓ, for different values of the impact angle φ and the separation s between injectors, is presented in Fig. 5. The behavior is almost linear for

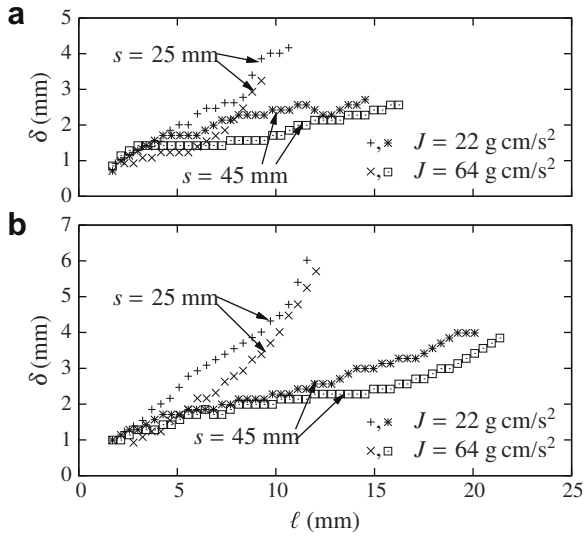

Fig. 5. Variation of δ with ℓ for different values of J and s. (a) $\varphi = 0°$; (b) $\varphi = 30°$.

small values of ℓ in all cases, which reflects that the straight line approximation can be still considered a valid approach, especially if the interaction between the opposed jets is negligible.

There can be observed a slight increase of the slope at high values of ℓ in the case $s = 25$ mm. This is due to the interaction with the incoming jet: since the distance between jets is small, the flow field generated by one of them is significantly disturbed by the other. A certain amount of bubbles coming from the opposed jet entrains to the zone of the outgoing jet, resulting in an increase of the number of bubble collisions and coalescence events in the central zone. This interaction between jets increases as the distance between them decreases, and in the case of $s = 45$ mm no considerable increase in the slope can be observed at the studied range of the momentum flux J, although it is expected to occur when using higher values of J. Data corresponding to $s = 45$ mm can be measured at higher values of ℓ than data corresponding to $s = 25$ mm, because when the injectors are far from each other, the interaction zone between the two colliding jets is located far from the outlet of the injector. It is also important to note that as J increases (with fixed values of φ and s), δ decreases, which is related to the fact that bubbles are smaller and they leave the injector outlet at high velocities, so they can reach higher distances from the nozzle before entering the bubbly plume zone.

Concerning the velocity field of the bubbly jet, it is necessary to take into account the bubble velocities and the liquid flow structure. As reported by Lima Neto et al. (2008b), the liquid velocity field differs from the motion of bubbles at a certain distance from the nozzle. In their work, both liquid velocity field and bubble properties were examined separately. It was observed that the water jet follows approximately the trajectory of the bubbles in the bubbly jet region, as inertial forces are much higher than buoyancy, and after some distance from the outlet the water jet partially separates from the bubble core. This leads to the assumption that, near the outlet of the nozzle, one can consider that bubbles are moving passively through the jet without perturbing significantly the flow field, where gravity forces can be neglected. Carrera et al. (2008) investigated the bubble velocities of bubbly jets in microgravity, and found that the motion of bubbles could be considered as passive tracers with respect to the carrier mean flow. To reinforce the basis of this approximation, the velocities of the bubbles at the jet centerline have been measured at $\varphi = 0°$, with two different values of the momentum flux J and different separations between injectors s. Averaging the velocities of five sample bubbles in each case, the variation of the velocity with the distance to the injector outlet has been obtained for $J = 22$ g cm/s^2 and $J = 54$ g cm/s^2, and is presented in Fig. 6a and b, respectively.

Following the procedure used by Carrera et al. (2008) to study the velocity of a bubbly jet in microgravity, we consider the Schlichting solution (Schlichting, 1979) for a single phase turbulent jet, where the x component of the velocity reads

$$v_x = \frac{3}{8\pi\varepsilon_0}\frac{J}{\rho_L}\frac{1}{(1+\eta^2/4)^2}\frac{1}{x}, \tag{4}$$

where $\varepsilon_0 = A_t/\rho_L$ is the virtual kinematic viscosity, A_t being the turbulent mixing coefficient, defined as the coefficient of proportionality between the Reynolds stress and the gradient of the mean velocity. The virtual kinematic viscosity is assumed constant over the whole of the jet (Schlichting, 1979), and

$$\eta = \frac{1}{4\varepsilon_0}\sqrt{\frac{3J}{\pi\rho_L}}\frac{y}{x}. \tag{5}$$

To avoid the divergence at $x = 0$, a parameter x_0 is introduced in order to take into account the finite size of the nozzle. In the jet centerline, $y = 0$, the modified equation becomes:

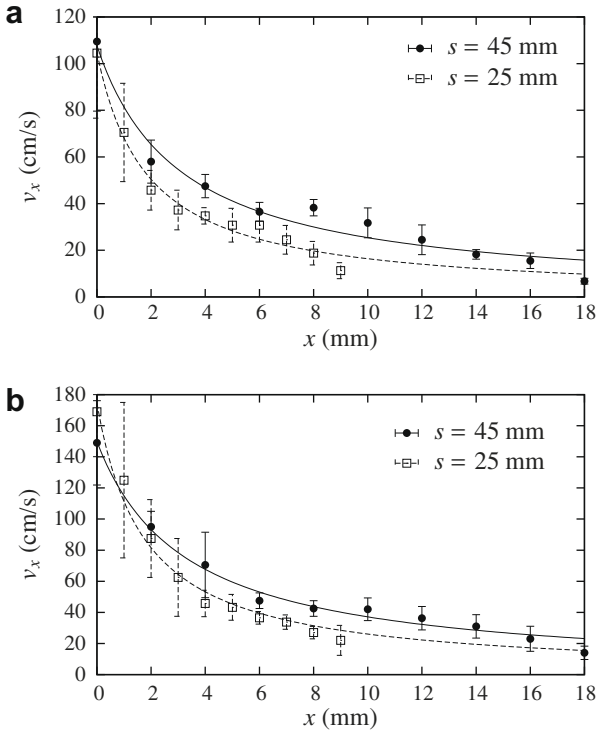

Fig. 6. Average bubble velocity at visual jet centerline. (a) $J = 22$ g cm/s^2; (b) $J = 54$ g cm/s^2. Fitted lines correspond to Eq. (6).

$$v_x = \frac{3}{8\pi\varepsilon_0}\frac{J}{\rho_L}\left(\frac{1}{x+x_0}\right) \equiv \theta(J)\frac{1}{x+x_0}. \tag{6}$$

The lines of Fig. 6a and b correspond to a fit of the measured velocities using Eq. (6). The values of the fitting parameters are shown in Table 1.

It can be observed in Fig. 6a and b that velocities corresponding to a separation between jets of $s = 25$ mm are lower than those corresponding to $s = 45$ mm for $J = 22$ g cm/s^2 and $J = 54$ g cm/s^2, respectively. This fact can be due to the interaction with the opposing jet: when s is small the jets are closer to each other and the flow field generated by the opposed jet can decrease the mean velocity in the jet centerline. This decrease in velocity should be larger at higher values of x. In fact we can observe that at large x, the measured velocity values are lower with respect to the fitting curves. Although there are only a few data points, this is a tendency which can be justified by considering the interaction with the opposed jet. We conclude that the presence of the opposed jet decreases the average jet velocity as bubbles reach the central zone where the two jets are colliding. The interaction between jets is thus not negligible and the velocity field can only be compared with that of a single injector at low values of x.

Except for a velocity scale, the structure of the turbulent liquid jet solution is independent of J. Consequently, all the velocity measurements of Fig. 6a and b should collapse on a single curve. In Fig. 7, we show a good fit of the measurements to the Schlichting

Table 1
Values of the fitting parameters θ and x_0.

J (g cm/s^2)	s (mm)	θ (cm^2/s)	x_0 (cm)
22	45	332 ± 33	3.1 ± 0.4
22	25	194 ± 14	1.9 ± 0.2
54	45	494 ± 29	3.3 ± 2.5
54	25	306 ± 22	1.8 ± 0.2

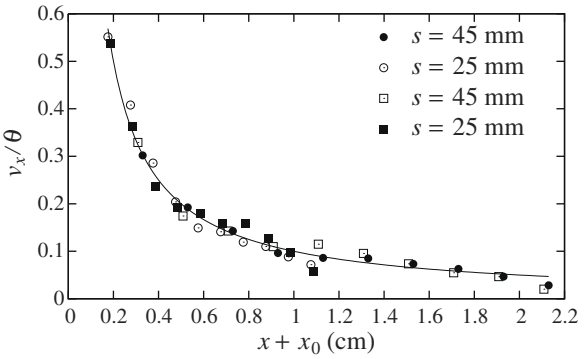

Fig. 7. Collapse of bubble velocity measurements. Circles and squares correspond to $J = 54$ g cm/s^2 and $J = 22$ g cm/s^2, respectively.

solution, which confirms the validity of considering bubbles as passive tracers near the nozzles.

For some industrial applications, it can be important to know the bubble spatial distribution in the bubbly plume zone, and how it changes when the jet strength, impact angles or separation are modified. In order to determine the bubble distribution, it is appropriate to measure the horizontal position (from now on, we will call x and y coordinates the horizontal and vertical position of a certain bubble, with respect to the left injector nozzle) of the bubbles when they are rising vertically. These measurements are related to the bubble motions inside the jets, and they can reflect which is the optimal jet configuration to achieve the most uniform bubble spatial distribution.

The method used to measure the probability for a bubble to rise in a determined x coordinate, consists of performing a line profile measure of a time averaged series of consecutive frames (see Fig. 8). The line profile measurements have been done at a height where almost all the bubbles rise vertically, and no more coalescences are expected to occur, so the distribution will not present considerable changes above this height. Following this procedure, a line profile measure has been carried out at a height of $h = 3$ cm from the injectors outlet for a series of 1000 consecutive frames (corresponding to $\Delta t = 1$ s). Two different values of the impact angle ($\varphi = 0°$ and 30°) have been considered in order to see the influence of the opposed jets orientation in the bubble spatial distribution. The data have been normalized to the number of bubbles that crossed that line to obtain the probability P_x that a bubble rise vertically in the coordinate x. The line profile measure has been done for two different values of the momentum flux ($J = 22$ g cm/s^2 and $J = 54$ g cm/s^2) and two values of the separation between injectors ($s = 25$ mm and $s = 45$ mm).

In Fig. 9a and b the probability P_x vs. the normalized distance x/s, at $\varphi = 0°$ and $\varphi = 30°$, respectively, are presented.

It can be observed that when using high values of the momentum flux J (this is, small bubbles), the probability for a bubble to rise in the central zone ($x/s \approx 0.5$) increases. In the case $s = 25$ mm and $J = 54$ g cm/s^2 the bubbles are widely dispersed in

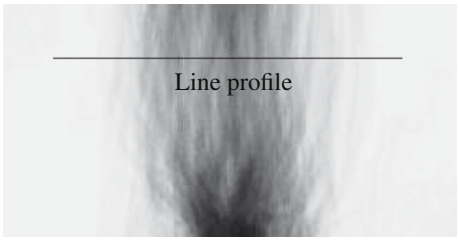

Fig. 8. Picture illustrating the line profile measurement method.

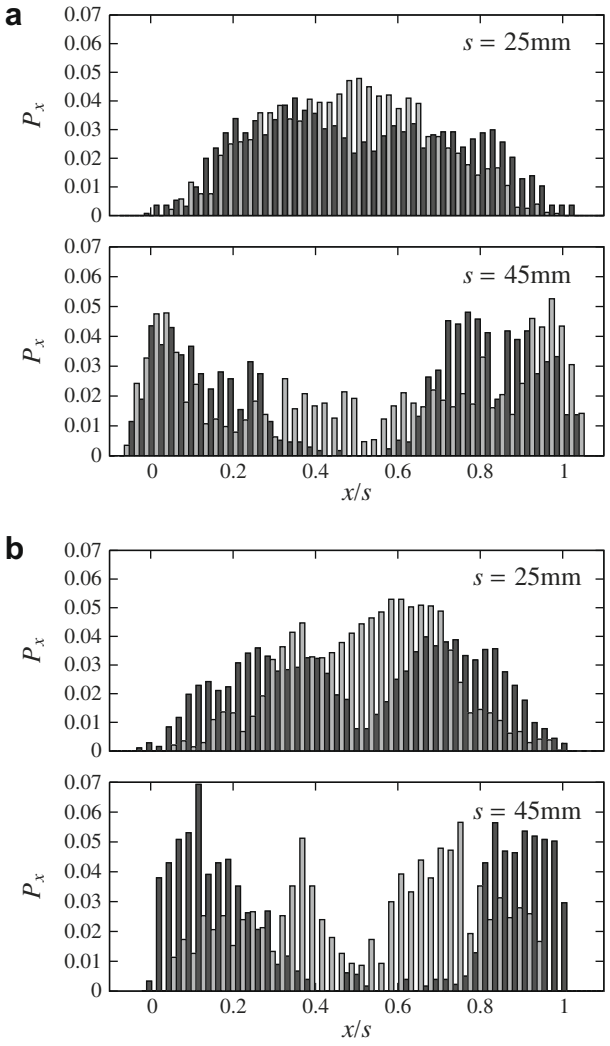

Fig. 9. P_x vs. x/s, for $J = 22$ g cm/s^2 (dark gray), and $J = 54$ g cm/s^2 (light gray). (a) $\varphi = 0°$; (b) $\varphi = 30°$.

the range $x \in (0,s)$, in both orientation angles $\varphi = 0°$ and $\varphi = 30°$. At fixed values of the momentum flux J, we observe that the bubbles are more uniformly distributed at $\varphi = 0°$ than in the case $\varphi = 30°$ in both situations $s = 25$ mm and $s = 45$ mm. This fact can be explained since there is a vertical component of the mean flow field when the orientation angle is different from zero. This upwards velocity, with the help of the flow field of the opposed jet, causes the bubbles to rebound and rise in a more enclosed region. This is in agreement with the results of Tsujimoto et al. (2006), who showed that the mixing efficiency of opposed jets increases at low impact angles. If the injectors are separated by $s = 45$ mm, the probability to rise in the central zone is nearly zero, especially in the case of $J = 22$ g cm/s^2, since in this case the jet strength is still not high enough to push the bubbles towards $x \approx s/2$. This is an indication that at low values of J, if the maximum distance that individual bubbles can reach along the jet axis is smaller than $s/2$, then the collisions of bubbles from different jets is not expected to occur, and no coalescences events will be encountered in the central zone. On the other hand, when the bubbles can reach distances of the order of $s/2$ or higher, the interaction between jets becomes important and the coalescences of bubbles from different jets can take place. In this situation, the interaction between jets

becomes important and the behavior of bubbles differs from that of an individual jet.

3.2. Bubble sizes and coalescence events

With the aim to know what is the order of magnitude of the bubble sizes we are dealing with, the diameters d_B of approximately 1000 bubbles have been obtained for two values of the momentum flux J. These diameters have been measured from 10 sample frames, with an automatic count of around 100 bubbles in each frame. Fig. 10 presents an histogram with the obtained results, where we can see that the sizes of the bubbles are in the same order of magnitude as the capillary diameter.

The dispersion in size of the bubbles is due to two facts: first, and most important, are the coalescence events. With the flow rates that have been used, multiple coalescences were observed in some bubbles, and this is the reason for the presence of this long tail in the diameter distribution. A more detailed discussion about coalescence is given at the end of this section. Second, is the fact that the injector has a little dispersion in the sizes of the bubbles generated, and this dispersion increases when high values of J are studied. This phenomenon is the reason why there are bubble diameters smaller than the capillary diameter, since no bubble breakups have been observed. It can be seen in Fig. 10 that the bubble diameters are smaller when $J = 64$ g cm/s^2, which is due to the higher amount of liquid flow rate used. In the studied range of injector operation, for any value of the liquid flow rate Q_L using low values of the gas flow rate Q_G, an increase of the gas flow rate results in an increase of the bubble generation frequency, and not on the bubble sizes. When the gas flow rate is higher than a certain critical value (about 10 ml/min for an injector of 1 mm diameter and $Q_L = 20$ ml/min), the generation frequency saturates and increasing Q_G leads to higher bubble diameters (Arias et al., 2009). The measured bubble size distribution is very similar to that obtained photographically by Varely (1995), although the sizes of the bubbles studied in his work ranged from 0.2 mm to 1 mm. Bubbly jets with mean bubble diameters between 1 mm and 5 mm were studied by Lima Neto et al. (2008a,b) and they also obtained a similar shape of the size distribution. Kamp et al. (2001) investigated the size of bubbles in bubbly flows through pipes (with bubble mean diameters ranging from 2 mm to 20 mm) and found distributions close to the present one, but with no such long tails due to the coalescence events, which occur very frequently after the bubbles have left the pipes creating therefore the bubbly jet.

It is possible that bubbles experience an expansion upon release into the tank due to the pressure difference between the capillary pressure and the tank pressure, which were not measured. In any case, since all bubbles have similar sizes (for fixed Q_L and Q_G), this expansion would be similar for all of them, and thus the peak in Fig. 10 would probably be slightly shifted to the right.

The CO_2 solubility in water could become an important factor in the bubble diameter determination. However, we have neglected the effects of solubility in bubble size since, according to Epstein and Plesset (1950), Ljunggren and Eriksson (1997), the lifetime of a CO_2 bubble of 1 mm diameter in water at our experimental conditions is of the order of several hours. Although our experiment runs for some minutes (between 2 and 5 min to ensure a steady state) before recording the high-speed sequence, a negligible amount of CO_2 is dissolved in water during this time. Moreover, the bubble diameter does not experience any significant change during the time interval (approximately 50 ms) in which the bubble enters the zone of observation and exits it. Thus, we consider that the concentration of CO_2 in water is steady in a time interval of 50 ms, which does not affect to the bubble diameter.

In order to have an image of the regions in the bubbly jets where the coalescence events take place, we have measured the (x,y) coordinates of such events that took place in $\Delta t = 0.2$ s. Fig. 11a and b show the positions of the coalescences that occurred for $J = 54$ g cm/s^2 with two values of the separation s and with $\varphi = 0°$ and $\varphi = 30°$, respectively. When $\varphi = 0°$ (Fig. 11a) and $s = 45$ mm, the coalescence locations are more or less uniformly dispersed, while in the case $s = 25$ mm the coalescence events occur more frequently and appear to be more concentrated in the central zone. This could be expected since the jet strength combined with the incoming flow of the opposed jet is forcing a high number of bubbles to collide.

It is important to note that some of the coalescence events occur near the injector outlet (see, for example, Fig. 11b). This fact, also observed by Carrera et al. (2008) using a single bubbly jet in microgravity, is due to a sudden decrease of velocity observed in some bubbles: when they have just detached from the nozzle they slow down drastically in an unexpected way. This decrease in

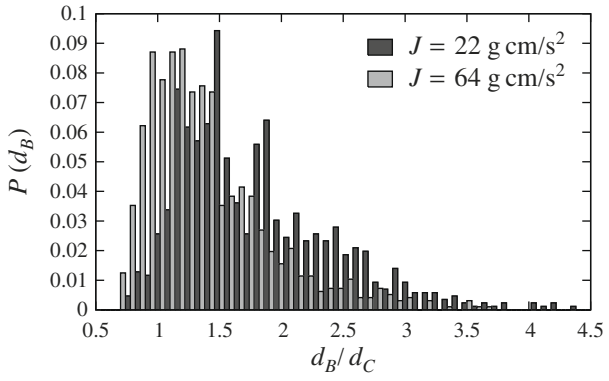

Fig. 10. Distribution of bubble diameters at $J = 22$ g cm/s^2 and $J = 64$ g cm/s^2.

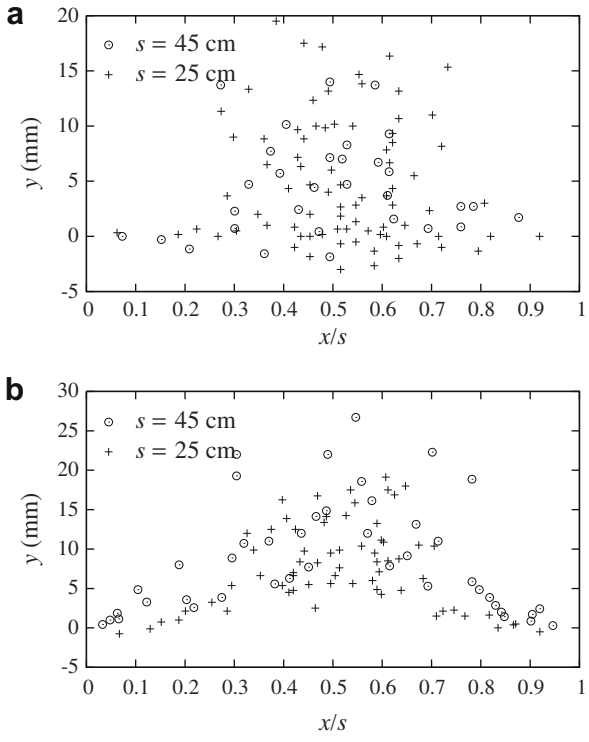

Fig. 11. Position of coalescence events in $\Delta t = 0.2$ s, for $J = 54$ g cm/s^2. (a) $\varphi = 0°$; (b) $\varphi = 30°$.

velocity facilitates the impact of the following bubble with the slow bubble, creating a larger bubble that, in turn, is more capable to coalesce since its size is larger and presents a higher cross section. From the movies recorded it is easy to see that when using high values of the gas flow rate Q_G and low values of the liquid flow rate Q_L (thus resulting a low value of the momentum flux J), the majority of the coalescence events occur just at the outlet of the nozzle. These coalescences are produced by bubbles from the same jet, since for low momentum fluxes bubbles are much higher in size and consequently slower. Only a small amount of coalescences are produced by bubbles coming from different jets, since bubble approach velocity is higher, and they take place in the central region where the opposed jets are colliding.

Finally, the coalescence probability P_{coal} vs. J has been studied at different orientation angles φ and separations s. The measurements have been carried out manually by following the bubbles individually frame by frame, counting the number of bubbles generated by the injectors and the number of coalescence events in a time interval of $\Delta t = 0.2$ s.

It can be observed in Fig. 12 that at low values of the momentum flux J, the number of coalescences is really high (nearly 70% of bubbles coalesce). This can be explained since the size of the generated bubbles is larger for low values of J, and larger bubbles suffer a decrease in their velocity just when they are in the outlet of the nozzle. A high diameter bubble moving slowly near the injector increases the probability to collide with the following bubble, and when this collision occurs, the size of the daughter bubble is even bigger increasing even more the coalescence probability. On the other hand, using high values of J the bubbles are smaller and they are injected at high velocities (around 100 cm/s), so the probability to collide with the following bubble is reduced drastically. The probability of coalescence at high values of J is still large, due to the fact that high-speed bubbles tend to collide with the bubbles of the incoming jet rather than with the preceding bubbles of the same jet. To clarify the ideas considered when creating the plot in Fig. 12, it should be noted that the coalescence probability has been measured considering that a coalescence is the collision of two bubbles creating a single larger daughter bubble, no matter if the coalescing bubbles have suffered any previous coalescences before. In fact, many bubbles can suffer coalescence more than once. An example of this is presented in Fig. 13, where a sequence of images with four bubbles coalescing into one large bubble (the smallest bubble do not coalesce) is shown. Four bubbles that coalesce into a single one, means that three coalescence events have been occurred using the definition already explained. The time interval between consecutive snapshots presented in Fig. 13 is 1 ms, meaning that the whole process takes place in 12 ms. The size of each snapshot is 42×43 pixels, corresponding to 6×6 mm approximately.

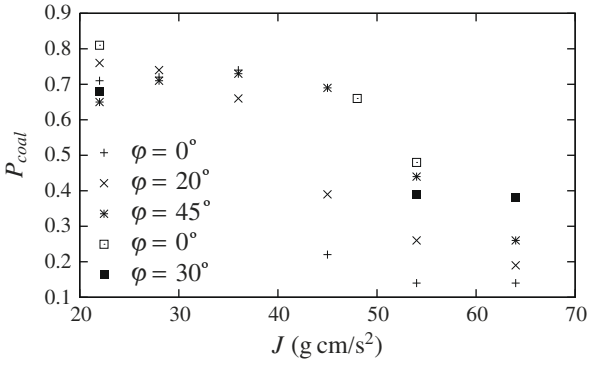

Fig. 12. Coalescence probability vs. J, at different angles φ and separations s. For the squares, $s = 25$ mm. For the rest, $s = 45$ mm.

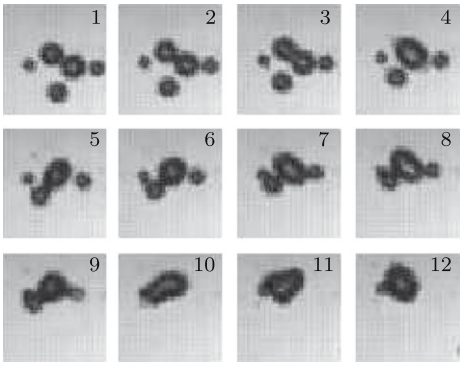

Fig. 13. Sequence of snapshots showing the coalescence process of four bubbles into a single daughter bubble.

4. Conclusions

We have designed an experimental setup for the study of bubble jet interactions and bubble coalescence on ground and in microgravity. The injection device can control bubble generation frequency, size and velocity, and the experimental apparatus permit us to modify the impact angle and separation between jets. We have presented on ground results concerning both the jet structure and bubble properties. The obtained results will be a reference for those to be obtained in a forthcoming drop tower campaign.

Two distinct regions of the bubbly jets have been observed. A first region where inertial and drag forces are predominant, gravity is negligible, and bubbles move passively through the turbulent liquid jet, and a second region where the bubbles rise vertically with constant velocity. The separation between these regions can be approximated as a line with constant slope, so the distance from the jet axis where the inertial forces are negligible increases linearly with the distance from the injection point. A substantial velocity decrease has been observed at the central zone of the opposed-jet configuration due to the strong interaction between the two jets. In the bubbly plume zone, where buoyancy is opposed to the drag force, bubbles appear to be more dispersed using larger values of the momentum flux and lower impact angles between jets. The sizes of the bubbles have been measured and diameters around 1 mm have been obtained. A large number of coalescence events occur at very short distances from the nozzle when using low values of the momentum flux, so the vast majority of the coalescences are produced by bubbles from the same jet. The coalescence probability is reduced considerably when increasing the momentum flux J.

The probability distribution P_x would certainly vary in microgravity depending on the height of the line profile. We expect to find a peak in P_x at the intersection between the two jets. We also expect to observe a global increase in P_{coal} in microgravity conditions. The reason for this is that in normal gravity the bubble average velocity is higher, while bubble collisions at higher relative velocity result in lower coalescence rates. Considering that the relative velocity between bubbles is smaller in microgravity, more coalescences would take place and P_{coal} would globally increase. Concerning the bubble diameter distribution in microgravity, we expect to find a similar form of the peak, which is mainly governed by the injector performance. Considering that there would be more

coalescences in low gravity conditions, this would result in a larger tail of the diameter distribution.

Further studies are required both in normal gravity and in microgravity conditions in order to get deeper insight into the role played by the gravity force on the bubbly jet structure. New methods that permit us to visualize separately the liquid flow are also necessary to quantify the deviation of the bubble trajectories from the liquid jet.

Acknowledgments

This work has been financially supported by the Spanish *Ministerio de Ciencia e Innovación* (Project AYA2009-11493). FS acknowledges financial support from *Comissionat per a Universitats i Recerca del Departament d'Innovació, Universitats i Empresa de la Generalitat de Catalunya i del Fons Social Europeu*.

References

Afanasyev, Y.D., Voropayev, S.I., Potylitsin, P.G., Filippov, I.A., 1995. Interaction of vortex dipoles: the theory and laboratory experiment. Atmos. Ocean. Phys. 30, 665–671.

Arias, S., Ruiz, X., Casademunt, J., Ramírez-Piscina, L., González-Cinca, R., 2009. Experimental study of a microchannel bubble injector for microgravity applications. Microgravity Sci. Technol. 21, 107–111.

Bhunia, A., Pais, S.C., Kamotani, Y., Kim, I.-H., 1998. Bubble formation in a coflow configuration in normal and reduced gravity. AIChE J. 44, 1499–1509.

Carrera, J., Ruiz, X., Ramírez-Piscina, L., Casademunt, J., Dreyer, M., 2008. Generation of a monodisperse microbubble jet in microgravity. AIAA J. 46, 2010–2019.

Chou, C.-P., Chen, J.-Y., Janicka, J., Mastorakos, E., 2004. Modeling of turbulent opposed-jet mixing flows with $\bar{\kappa}$–$\bar{\epsilon}$ model and second order closure. Int. J. Heat Mass Transfer 47, 1023–1035.

Eckestein, J.-Y., Chen, J., Chou, C.-P., Janicka, J., 2000. Modeling of turbulent mixing in opposed jet configuration: one-dimensional monte carlo probability density function simulation. Proc. Combust. Inst. 28, 141–148.

Epstein, P.S., Plesset, M.S., 1950. On the stability of gas bubbles in liquid–gas solutions. J. Chem. Phys. 18, 1505–1509.

Eren, H., 2006. Numerical study of unsteady interacting compressible jet flows using finite difference method for small Reynolds numbers. Appl. Math. Comput. 172, 876–891.

Gabriel, K.S., 2007. Microgravity two-phase flow and heat transfer. Space Technology Library, vol. 19. Springer.

Jianfu, Z., Jingchang, X., Hai, L., Wenrui, H., Ivanov, A.V., Belyaev, A.Y., 2000. Microgravity experiments of two-phase flow patterns aboard MIR space station. Acta Mech. Sinica 17, 151–159.

Kamp, A.M., Chesters, A.K., Colin, C., Fabre, J., 2001. Bubble coalescence in turbulent flows: a mechanistic model for turbulence-induced coalescence applied to microgravity bubbly pipe flow. Int. J. Multiphase Flow 27, 1363–1396.

Kim, I., Kamotani, Y., Ostrach, S., 1994. Modeling bubble and drop formation in flowing liquids in microgravity. AIChE J. 40, 19–28.

Lima Neto, I.E., Zhu, D.Z., Rajaratnam, N., 2008a. Bubbly jets in stagnant water. Int. J. Multiphase Flow 34, 1130–1141.

Lima Neto, I.E., Zhu, D.Z., Rajaratnam, N., 2008b. Horizontal injection of gas–liquid mixtures in a water tank. J. Hydraul. Eng. 134, 1722–1731.

Ljunggren, S., Eriksson, J.C., 1997. The lifetime of a colloid-sized gas bubble in water and the cause of the hydrophobic attraction. Colloids and Surf. A: Physicochem. Eng. Aspects, 151–155.

Nahra, H.K., Kamotani, Y., 2003. Prediction of bubble diameter at detachment from a wall orifice in liquid cross-flow under reduced and normal gravity conditions. Chem. Eng. Sci. 58, 55–69.

Ohta, H., Baba, A., Gabriel, K.S., 2002. Review of existing research on microgravity boiling and two-phase flow. Future Experiments on the International Space Station. Ann. NY Acad. Sci. 974, 410–427.

Schlichting, H., 1979. Boundary-Layer Theory, seventh ed. McGraw-Hill Classic Textbook Reissue, New York.

Suñol, F., Maldonado, O., Pino, R., González-Cinca, R., 2009. Design of an experiment for the study of bubble jet interactions in microgravity. Microgravity Sci. Technol. 21, 95–99.

Tsuge, H., Terasaka, K., Koshida, W., Matsue, H., 1997. Bubble formation at submerged nozzles for small gas flow rate under low gravity. Chem. Eng. Sci. 52, 3415–3420.

Tsujimoto, K., Shakouchi, T., Sasazaki, S., Toshitake, A., 2006. Direct numerical simulation of jet mixing control using combined jets. JSME Int. J., Ser. B 49, 966–973.

Varely, J., 1995. Submerged gas–liquid jets: bubble size prediction. Chem. Eng. Sci. 50, 901–905.

Voropayev, S.I., Afanasyev, Y.D., 1992. Two-dimensional vortex–dipole interactions in a stratified fluid. J. Fluid Mech. 236, 665–689.

Voropayev, S.I., Afanasyev, Y.D., Korabel, V.N., Filippov, I.A., 2003. On the frontal collision of two round jets in water. Phys. Fluids 15, 3429–3433.

Weifeng, L., Zhigang, S., Haifeng, L., Fuchen, W., Zunhong, Y., 2008. Experimental and numerical study on stagnation point offset of turbulent opposed jets. Chem. Eng. J. 138, 283–294.